Dynamic Localization of Trypanosoma brucei Mitochondrial DNA Polymerase ID

Article *in* Eukaryotic Cell · January 2012

DOI: 10.1128/EC.05291-11 · Source: PubMed

3 authors, including:

Michele Klingbeil
University of Massachusetts Amherst
32 PUBLICATIONS **1,448** CITATIONS

SEE PROFILE

EC
Journals.ASM.org

Dynamic Localization of *Trypanosoma brucei* Mitochondrial DNA Polymerase ID

Jeniffer Concepción-Acevedo, Juemin Luo, and Michele M. Klingbeil

Department of Microbiology, University of Massachusetts, Amherst, Massachusetts, USA

Trypanosomes contain a unique form of mitochondrial DNA called kinetoplast DNA (kDNA) that is a catenated network composed of minicircles and maxicircles. Several proteins are essential for network replication, and most of these localize to the antipodal sites or the kinetoflagellar zone. Essential components for kDNA synthesis include three mitochondrial DNA polymerases TbPOLIB, TbPOLIC, and TbPOLID). In contrast to other kDNA replication proteins, TbPOLID was previously reported to localize throughout the mitochondrial matrix. This spatial distribution suggests that TbPOLID requires redistribution to engage in kDNA replication. Here, we characterize the subcellular distribution of TbPOLID with respect to the *Trypanosoma brucei* cell cycle using immunofluorescence microscopy. Our analyses demonstrate that in addition to the previously reported matrix localization, TbPOLID was detected as discrete foci near the kDNA. TbPOLID foci colocalized with replicating minicircles at antipodal sites in a specific subset of the cells during stages II and III of kDNA replication. Additionally, the TbPOLID foci were stable following the inhibition of protein synthesis, detergent extraction, and DNase treatment. Taken together, these data demonstrate that TbPOLID has a dynamic localization that allows it to be spatially and temporally available to perform its role in kDNA replication.

Mitochondrial DNA (mtDNA) is packaged into protein-DNA complexes called nucleoids. These structures are dynamic macrocomplexes located in the mitochondrial matrix, and they act as units of mtDNA replication and inheritance with composition that can undergo remodeling in response to metabolic stresses (7, 23, 47). Using bromodeoxyuridine (BrdU) incorporation, nucleoids have been shown to be the sites of mtDNA replication in yeast and mammalian cells (35, 39). However, not all nucleoids replicate concurrently; only a subset undergo replication at any given time. With no strict control related to cell cycle progression, the segregation and inheritance of the nucleoid depends upon a membrane-associated apparatus that interacts with the fusion and fission machinery of the mitochondrial organelle network (2, 19, 31). Lastly, while the protein composition of nucleoids varies among cell types and in response to metabolic conditions, the core proteins of the nucleoid appear to remain constant and include transcription and replication factors, such as mitochondrial transcription factor A, single-stranded binding protein, Twinkle helicase, and the sole mitochondrial DNA polymerase, Pol γ (1, 21).

One of the most unusual and structurally complex mtDNA genomes is found in trypanosomatid parasites such as *Trypanosoma brucei*, the causative agent of African sleeping sickness. This extranuclear genome, called kinetoplast DNA (kDNA), is a network composed of thousands of topologically interlocked minicircles and maxicircles that are condensed into a single disk-shaped nucleoid structure. Approximately 25 identical maxicircle copies (23 kb) encode a subset of respiratory chain subunits and rRNA, similarly to other eukaryotic mtDNA. However, several cryptic maxicircle transcripts require posttranscriptional RNA editing (insertion and/or deletion of uridine residues) to generate functional open reading frames. RNA editing depends upon guide RNAs (gRNAs) encoded on the heterogeneous population of 5,000 minicircles (1 kb) (49). Therefore, the coordinated replication of both minicircles and maxicircles is essential for mitochondrial physiology and parasite survival.

Key features of the kDNA replication mechanism include replication once per cell cycle in near synchrony with nuclear S phase, a topoisomerase II-mediated release and reattachment of minicircles, and a multiplicity of DNA polymerases (six), helicases (six), and primases (two) for kDNA transactions (17, 18, 22, 27, 45). Briefly, covalently closed minicircles are released from the network into the kinetoflagellar zone (KFZ), a specialized region between the kDNA disk and the mitochondrial membrane nearest the basal body (bb) (10). The free minicircles initiate unidirectional theta structure replication primarily through interactions with proteins such as universal minicircle sequence binding protein (UMSBP) and p38 (26, 33). TbPOLIB and TbPOLIC also localize to this region. Minicircle progeny (still containing at least one gap) are subsequently reattached at two electron-dense areas positioned 180° apart at the network periphery called the antipodal sites. Several proteins associated with Okazaki fragment processing and reattachment to the network localize to the antipodal sites, including SSE1, DNA Pol β, DNA ligase kβ (Ligk β), and topoisomerase II (Topo II_{mt}) (9, 12, 20, 43, 50). As a result, there is spatial and temporal separation of replication events with early initiation occurring in the KFZ, followed by Okazaki fragment processing and reattachment at the antipodal sites. Reattachment occurs before all gaps have been filled. Once all minicircles have replicated, the gapped molecules undergo a final phase of gap filling, presumably by Pol β-PAK and DNA ligase kα. Far less is known about maxicircle replication. In contrast to minicircles, maxicircles remain catenated to the network during replication, accumulate at the center of a growing disk, and are the last molecules to segregate (14). Currently, only two proteins have been

Received 18 November 2011 **Accepted** 21 January 2012

Published ahead of print 27 January 2012

Address correspondence to Michele M. Klingbeil, klingbeil@microbio.umass.edu.

Supplemental material for this article may be found at http://ec.asm.org/.

doi:10.1128/EC.05291-11

shown to be essential for maxicircle replication, a DNA helicase (TbPIF2) and a primase (PRI1) (17, 27). Thus far, the main maxicircle replicase has not been described.

In the cell's single mitochondrion, the kDNA is positioned within the mitochondrial matrix near the flagellar bb. kDNA S phase occurs almost in synchrony with bb duplication. Additionally, kDNA segregation and positioning are dependent on bb movement and separation. Failure to segregate the bb results in impaired network segregation, providing additional evidence for the link between bb segregation and kDNA division (16, 40). A filament system called the tripartite attachment complex (TAC) physically links the bb and the kDNA (38, 41). The disruption of the two known TAC proteins by the depletion of p166 and overexpression of a dominant-negative form of AEP-1 causes impaired kDNA segregation (37, 52). The kinetoplast duplication cycle is characterized by morphological differences that can be divided into five distinct stages (14). At stage I, cells contain 1 kDNA disk, no visible antipodal sites, and 1 basal body/probasal body (bb/pro-bb) pair. During stages II and III, the kDNA transitions from a bilobed to a V-shaped structure, and both stages contain 2 bb/pro-bb pairs as well as antipodal sites. The segregation of the replicated kDNA network initiates during stage IV. Networks remain connected by a thread of maxicircles that is resolved in stage V when both networks are morphologically the same as in stage I. In both stages (IV and V), 2 bb/pro-bb pairs are observed and antipodal sites are not detected.

The spatial and temporal localization of kDNA replication proteins likely is important for their participation in this highly coordinated and dynamic process. So far, a majority of kDNA replication proteins localize mainly to the KFZ and the antipodal sites. Since the discovery of the first antipodal kDNA replication protein, Topo II_{mt} (32), many more proteins share a pattern of antipodal localization. It has been proposed that the composition of proteins at the antipodal sites is dynamic, and the localization of some of these proteins to the antipodal sites seems to be periodic (20, 46). Initial localization studies of the three essential mitochondrial DNA polymerases indicated that TbPOLIB and TbPOLIC localized to the KFZ, while TbPOLID was distributed throughout the mitochondrial matrix (22). The matrix localization of TbPOLID suggests that this protein redistributes close to the kDNA network or is needed in very low abundance to perform its role in kDNA replication. Using a POLID-PTP-tagged single expressor cell line (PTP stands for protein C-tobacco etch virus-protein A) and immunofluorescence microscopy (IF), we characterized in detail the dynamic localization of TbPOLID during the *T. brucei* cell cycle. Here, we describe a detailed localization pattern for TbPOLID in which the protein accumulates as foci during stages II and III of the kDNA S phase and becomes dispersed throughout the mitochondrial matrix at all other cell cycle stages. We provide evidence that TbPOLID changes in localization occur through a mechanism that involves the redistribution of the mitochondrial matrix fraction to the antipodal sites. Taken together, these data demonstrate that TbPOLID is spatially and temporally available to perform its essential role in kDNA replication.

MATERIALS AND METHODS

Chromosomal tagging and single-allele deletion. (i) pPOLID-PTP-NEO. *TbPOLID* C-terminal coding sequence (1,635 bp) was PCR amplified from *T. brucei* 927 genomic DNA using forward (5′-ATA ATA GGG CCC TGC TCG TCA AGA GGT GCG-3′) and reverse (5′-ATA ATA CGG CCG CAG TGT CTC CTC AAT GAC AAC G-3′) primers containing ApaI and EagI sites, respectively. The PCR-amplified fragment was ligated into ApaI and NotI restriction sites of pC-PTP-NEO (44) to create the pPOLID-PTP-NEO vector.

(ii) POLID knockout construct pKOPOLID^{Puro}. pKO^{Puro} is a derivative of the pKO$^{NEO/HYG}$ series (24) and was a gift from Paul Englund (34). A 629-bp *TbPOLID* 5′-untranslated region (UTR) fragment was PCR amplified using forward (5′-CTC GAG CAG GGA AAG ATA GCG CCT-3′) and reverse (5′-ATC GAT AAA AAG AAG GAT GCG-3′) primers containing XhoI and ClaI sites, respectively, and ligated into pKO^{Puro}. Subsequently, a 483-bp *TbPOLID* 3′ UTR fragment was PCR amplified using forward (5′-ACT AGT GTG TCC TAT AGC AGT AAC G-3′) and reverse (5′-GCG GCC GCA GCA ATT TTC CGC AC-3′) primers containing SpeI and NotI sites, respectively, and ligated into SpeI and NotI sites in the downstream polylinker portion of the pKO^{Puro} vector to generate the pKOPOLID^{Puro} construct. After digestion with XhoI and NotI, the 3,359-bp fragment containing the puromycin resistance marker flanked by the POLID UTRs was used for transfection into parasites.

(iii) Myc tagging of TbPIF2. The original pPIF2-myc construct (27) (a generous gift from Paul Englund) was modified to create the pPIF2-Myc-BLA construct. Briefly, we modified this vector by replacing the neomycin resistance marker with the blasticidin resistance marker from the pMOtag2H vector (36) using HindIII and BamHI digestion.

Trypanosome growth and transfection. Procyclic *T. brucei* strain Lister 427 was cultured at 27°C in SDM-79 containing 15% heat-inactivated serum and was transfected by electroporation with SnaBI-linearized pPOLID-PTP-NEO (10 μg). A stable population was first selected with 50 μg/ml G418, followed by limiting dilution as described previously (4, 6), resulting in a plating efficiency of 70%. Clonal cell line TbID-PTP P2B7 then was transfected with XhoI/NotI-digested pKOPOLID^{Puro} vector (15 μg/ml), and the population was selected with 50 μg/ml G418 and 1 μg/ml puromycin (Puro). Following limiting dilution cloning, a plating efficiency of 44% was obtained, and clonal cell lines were analyzed for POLID-PTP expression and proper chromosomal integration by Western and Southern blot analyses, respectively. Three individual clones were analyzed for growth rate and potential defects in kDNA morphology. For each clone, the doubling time was ~9 h, which is similar to the 427 parental cell line, and no detectable defects in kDNA morphology were observed following DAPI staining. The data presented in this study correspond to clonal cell line POLID-PTP/IDKO^{Puro} P2H7, which we named TbID-PTP. For the cycloheximide (CHX) experiments (see below), TbID-PTP was transfected with the pPIF2-Myc-BLA construct to generate a coexpressing cell line.

Immunofluorescence. TbID-PTP cells were harvested for 5 min at 1,000 × *g*, resuspended in cytomix, and adhered to poly-L-lysine (1:10)-coated slides for 5 min. Cells were fixed for 5 min using 4% paraformaldehyde and washed three times (5 min each) in phosphate-buffered saline (PBS) containing 0.1 M glycine (pH 7.4) followed by methanol permeabilization (overnight, −20°C). Cells then were washed in PBS 3 times for 5 min, followed by incubation with anti-protein A serum (Sigma) and rat monoclonal antibody YL1/2 (Abcam) together for 90 min and diluted 1:5,000 and 1:400, respectively, in PBS containing 1% bovine serum albumin (BSA). Cells then were washed 3 times in PBS containing 0.1% Tween 20 and incubated with the secondary antibodies (60 min) Alexa Fluor 594 goat anti-rabbit and Alexa Fluor 488 goat anti-rat, both diluted 1:250 in PBS containing 1% BSA. DNA was stained with 3 μg/ml 4′-6′-diamidino-2-phenylindole (DAPI), and slides were washed 3 times in PBS prior to mounting in Vectashield (Vector Laboratories). The immunolabeling of exclusion zone filaments using monoclonal antibody (MAb) 22 was performed as described in reference 3.

***In situ* TdT labeling.** Cells were fixed in paraformaldehyde, permeabilized in methanol, and labeled with terminal deoxynucleotidyl transferase (TdT) as previously described (20, 26). Briefly, cells were rehydrated in PBS and incubated for 20 min at room temperature in 25 μl of

1× TdT reaction buffer (Roche Applied Science) containing 2 mM $CoCl_2$. Cells then were labeled for 60 min at room temperature in a 25-μl reaction solution (1× TdT reaction buffer, 2 mM $CoCl_2$, 10 μM dATP, 5 μM Alexa Fluor 488-dUTP, and 40 U of TdT). The reaction was stopped by the addition of 2× SSC (1× SSC is 0.15 M NaCl plus 0.015 M sodium citrate). Slides were processed for the immunolocalization of PTP-tagged protein as described above.

Immunofluorescence microscopy of detergent-extracted and DNase-treated cells. (i) Detergent extraction. Cells were adhered to poly-L-lysine-coated slides (5 min), extracted for 5 min in NP-40 buffer (0.25% NP-40, 10 mM Tris-HCl, 1 mM $MgCl_2$, pH 7.4), fixed in 4% paraformaldehyde, and then processed with our standard TdT labeling and immunofluorescence protocol as described above. To confirm POLID-PTP foci resistance to detergent extraction, we also performed extractions using 1% NP-40 (5 min) and observed the presence or absence of POLID-PTP foci by IF.

(ii) DNase and RNase treatment. Detergent-extracted cells were incubated for 60 min with 10 U of DNase I (NEB), washed 3 times in 1× PBS, and fixed in 4% paraformaldehyde. Slides then were processed for the immunolocalization of PTP-tagged protein as described above. For RNase treatment, detergent-extracted cells were incubated with 60 μg of RNase A (Invitrogen) for 20 min prior to fixation and immunodetection.

Image analysis and quantification. (i) Microscope and software. Images were acquired with a Nikon Eclipse E600 microscope using a cooled charge-coupled-device Spot-RT digital camera (Diagnostic Instruments) and a 100× Plan Fluor 1.30-numeric-aperture (oil) objective. Brightness and contrast were adjusted for all images using Adobe Photoshop CS4.

(ii) Measurements of basal body distance. Cells were labeled with YL1/2 and anti-protein A for bb and POLID-PTP detection, respectively. The distance between bb was measured in 149 cells from randomly selected fields using the Spot Imaging Solution software (Diagnostic Instruments). These cells were classified based on their kDNA morphology and the presence or absence of POLID-PTP foci.

(iii) FI calculation. Fluorescence intensity (FI) was determined using Image J software (http://imagej.nih.gov/ij/). The freehand selection tool was used to determine the total FI of whole cells that were focus positive (WC). The oval selection tool was used to measure the FI of independent foci (see Fig. S2 in the supplemental material for examples). To determine the net FI of the mitochondrial matrix (MM), we subtracted the FI of the foci from the FI of WC (equation 1, numerator). The same principle was used to determine the net area of the mitochondrial matrix (equation 1, denominator). Therefore, equation 1 shows the net FI of the MM.

$$\text{Net FI}_{\text{MM}} = \frac{\text{FI}_{\text{WC}} - \sum_{i=1}^{n} \text{FI}_{\text{foci}}}{\text{Area}_{\text{WC}} - \sum_{i=1}^{n} \text{Area}_{\text{foci}}} \quad (1)$$

To obtain the fold increase within an individual focus, we calculated the ratio of focus FI to net FI of the MM. Background subtraction was performed on all images using the Spot Imaging Solution software (Diagnostic Instruments). Standard errors of the means (SEM) were determined by analyzing the FI from 10 different cells. Analysis of SEM was performed using GraphPad Prism version 5.00 for Mac OS X (GraphPad Software, San Diego, CA).

(iv) TdT labeling quantification. Only intact cells identified by differential interference contrast (DIC) were included in the analysis. More than 300 cells were scored from three separated experiments (~1,000 total cells). Early and late TdT-positive cells were classified as $1N1K_{div}$ cells, and TdT-negative cells were classified based on the kDNA morphology observed by DAPI staining. The numbers of POLID-PTP foci were distinguished by focusing up and down through several focal planes. Cells with three foci were hard to distinguish from 2-foci cells due to the distance between each focus, and therefore they may be underrepresented in this analysis.

Western blotting. Parasites were harvested at 3,500 × *g* for 10 min (4°C), and cell pellets were washed once in PBS supplemented with protease inhibitor cocktail set III (1:100) (CalBioChem). Cells were lysed in 4× SDS sample buffer containing 5% beta-mercaptoethanol and incubated at 94°C for 4 min. Proteins were separated by SDS-PAGE and transferred to polyvinylidene difluoride (PVDF) membrane overnight at 90 mA in transfer buffer containing 0.1% methanol. The membrane was incubated in 1% Roche blocking reagent (60 min) followed by incubation with antibodies diluted in 0.5% blocking reagent (60 min). PTP-tagged protein was detected with 1:2,000 peroxidase-anti-peroxidase soluble complex (PAP) reagent (Sigma), which recognizes the protein A domain of the PTP tag. For additional antibody detections, the membrane was stripped for 15 min with 0.1 M glycine (pH 2.5), washed in Tris-buffered saline (TBS) with 0.1% Tween 20, blocked, and reprobed with *Crithidia fasciculata*-specific Hsp70 antibody (1:10,000) (11) followed by secondary chicken anti-rabbit IgG-horseradish peroxidase (HRP) (1:10,000) or *T. brucei* anti-Pol β (1:1,000) (43), followed by anti-rat antibody (1:5,000). The detection of PIF2-Myc was done using anti-Myc (1:1,000) from Santa Cruz followed by secondary goat anti-mouse (1:1,000). BM chemiluminescence Western blotting substrate (POD) from Roche was used for protein detection.

CHX treatment. A cell line coexpressing POLID-PTP and PIF2-Myc was incubated for 6 h with 100 μg/ml CHX. Cells were harvested every hour and processed for Western blot analysis or processed for the immunolocalization of PTP-tagged protein as described above.

RESULTS

POLID is detected as discrete foci. The majority of kDNA replication proteins studied localize to specific regions surrounding the kDNA, mainly the antipodal sites and the KFZ (17, 18, 28, 29, 45). Previously, we demonstrated that TbPOLID is one of three mitochondrial DNA polymerases that are essential for parasite survival and the maintenance of the kDNA network (6). However, the initial localization of TbPOLID using a peptide antibody showed that it was distributed throughout the mitochondrial matrix (22), suggesting that POLID would need to redistribute to the kDNA disk to perform its essential role in kDNA replication. To investigate the localization of TbPOLID in detail, we generated an exclusive expresser cell line, TbID-PTP, in which one *TbPOLID* allele was deleted and the remaining allele was fused to the PTP sequence by the targeted integration of the construct pPOLID-PTP-NEO (Fig. 1A). The expected-size product of POLID-PTP (~200 kDa) was detected in all 17 clonal cell lines by Western blotting using PAP antibody (data not shown). The integration of both events was confirmed by Southern blot analysis (data not shown), and three of the clones with proper integration were selected for detailed characterization. The PTP tag was detected only in TbID-PTP whole-cell extracts with no cross-reactivity observed in 427 wild-type (WT) whole-cell extracts (Fig. 1B). The growth rate was analyzed in the three TbID-PTP clones, and each cell line had a doubling time of ~9 h, which is similar to that of the 427 parental cell line, and had no detectable defects in kDNA morphology, as shown by DAPI staining (Fig. 1C). TbPOLID is essential for cell growth and kDNA replication, thus our data indicate that the PTP tag does not impair the essential function of this protein. The fluorescence microscopy of TbID-PTP clonal cell lines revealed localization throughout the mitochondrial matrix as previously described. In addition, we detected a new localization pattern in a subpopulation of the cells, where POLID-PTP was present as discrete fluorescent spots at regular positions, always in close proximity with the kDNA disk (Fig. 1C). Cells containing POLID-PTP foci displayed decreased mitochondrial matrix fluorescent signal. The results obtained were very similar for

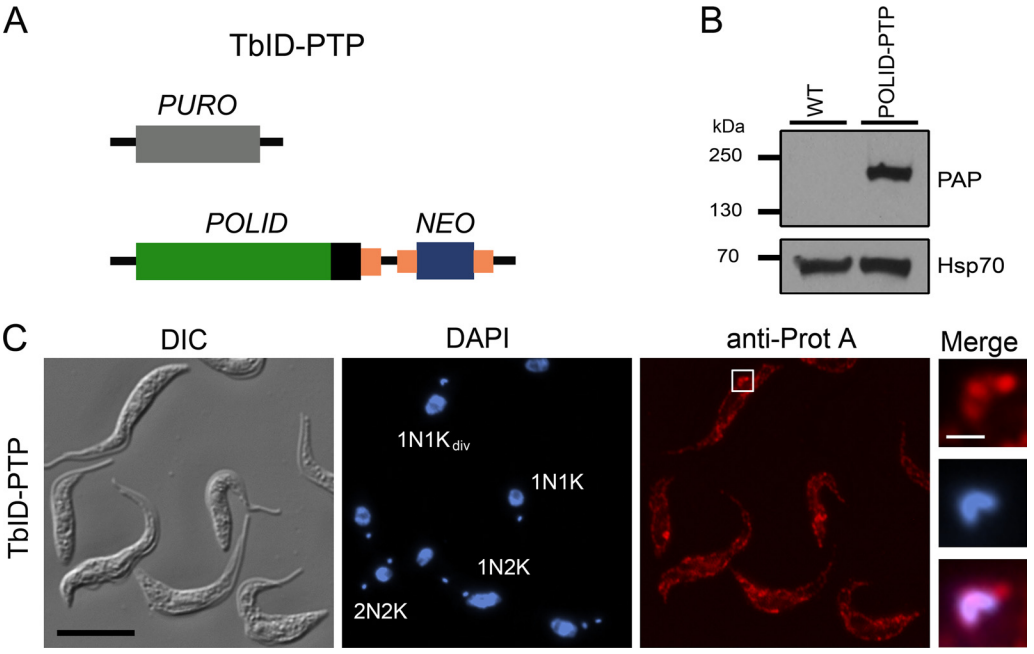

FIG 1 POLID-PTP exclusive expressing cell line. (A) Diagrammatic representation (not to scale) of the *TbPOLID* gene locus in clonal cell line TbID-PTP. The *TbPOLID* coding region (green) was replaced in one allele by a puromycin resistance gene (PURO), and in the second allele the PTP sequence was fused to the 3′ end of the coding region by the targeted insertion of the pPOLID-PTP-NEO construct. Coding regions of selectable marker genes are indicated by a gray box (PURO) and blue box (NEO). The PTP sequence is indicated by a black box and introduced gene-flanking regions by small orange boxes. (B) Immunoblot analysis of whole-cell extracts of wild-type (WT) and TbID-PTP cells. A total of 5×10^6 cells were loaded per lane, and tagged protein was detected with PAP reagent (top panel). The same blot was stripped and reprobed with Hsp70 antibody as a loading control. (C) Localization of POLID-PTP in an unsynchronized population. POLID-PTP was detected using anti-protein A (red), and DNA was stained with DAPI (blue). Panels in the merge column are enlargements of the area indicated by the white square. Scale bar sizes are 10 and 1 μm, respectively.

all three clones (data not shown), and only the data for clone P2H7 are shown in this study.

POLID-PTP foci are stable. The appearance of POLID-PTP foci in a subpopulation of the cells suggests that POLID undergoes redistribution from the mitochondrial matrix to the kDNA disk. Alternatively, changes in protein abundance also could account for this variation in POLID-PTP localization. The only mitochondrial protease that has been shown to regulate kDNA replication is TbHslVU (25). This bacterial-like protease regulates maxicircle replication through the degradation of the helicase TbPIF2 (27). To determine if proteolytic degradation plays a role in the regulation of POLID-PTP localization patterns, we inhibited protein synthesis using 100 μg/ml of CHX during a time course of 6 h. For this experiment we generated a cell line coexpressing POLID-PTP and PIF2-Myc, and we monitored protein levels by immunoblotting.

Additionally, POLID-PTP foci formation was monitored by immunofluorescence. As expected, PIF2-Myc levels decreased to undetectable levels after 2 h of CHX treatment (Fig. 2A). However, POLID-PTP protein levels remained unchanged during CHX treatment, which is similar to results of treatment with Pol β, which is not regulated by proteolytic degradation (Fig. 2A, first and third panels). These data suggest that POLID is a stable protein and is not regulated by proteolytic degradation. We next investigated whether the accumulation of POLID-PTP foci was dependent upon new protein synthesis. After 2, 4, and 6 h of CHX treatment, cells were fixed and analyzed for POLID-PTP localization (Fig. 2B). At each time point, we detected POLID-PTP foci in a subpopulation of the cells, demonstrating that the foci are stable and that their formation was not dependent on newly synthesized protein.

POLID-PTP has a dynamic localization during the cell cycle. bb duplication occurs almost simultaneously with the initiation of kDNA S phase (51). Importantly, multiple studies have demonstrated that bb duplication and positioning are tightly linked with kinetoplast replication and segregation (14, 41, 42). bb duplication events and inter-bb distance are easily monitored by light microscopy, providing a marker for early and late events of the *T. brucei* kDNA S phase. To precisely determine if the appearance of POLID-PTP foci is coordinated with cell cycle progression, we monitored POLID-PTP localization in relation to bb duplication events. Basal bodies were labeled using the monoclonal antibody YL1/2, which detects the tyrosinated form of the alpha-tubulin subunit. Cells with one kDNA network had a single bb/pro-bb pair, and the localization of POLID-PTP was dispersed throughout the mitochondrial matrix (Fig. 3A, 1N1K cells). When cells transition from 1N1K to $1N1K_{div}$ (cells undergoing kDNA replication), an additional signal corresponding to the new bb was detected and POLID-PTP is observed as discrete foci close to the kDNA disk in a majority of the $1N1K_{div}$ cells (Fig. 3A, $1N1K_{div}$, focus positive and negative). The $1N1K_{div}$ cells with bb positioning farther apart (indicating a later stage in cell cycle progression) had POLID-PTP localized throughout the mitochondrial matrix (Fig. 3A, $1N1K_{div}$, focus negative). The matrix localization pattern persisted in cells with two bb signals associated with two newly segregated kDNA networks (1N2K) and cells that were undergoing cytokinesis (2N2K). These data demonstrate that POLID-PTP

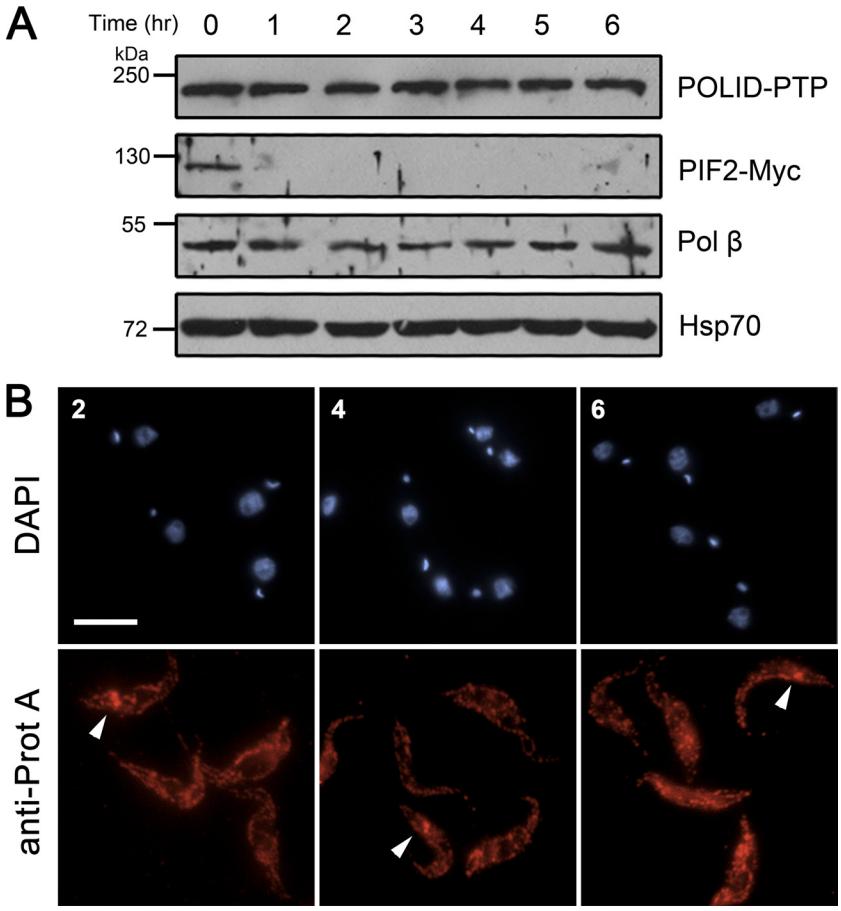

FIG 2 POLID-PTP protein levels and foci formation after CHX treatment. (A) Western blot detection of POLID-PTP, PIF2-Myc, Pol β, and Hsp70 protein levels following CHX treatment. Cells were harvested every hour, and 5×10^6 cells were loaded into each well. (B) Immunofluorescence detection of POLID-PTP foci following CHX treatment. Cells were fixed at 2-, 4-, and 6-h intervals and stained/labeled with DAPI (blue) and anti-protein A (red). POLID-PTP foci are indicated by arrows. Scale bar, 10 μm.

accumulates as foci during kDNA S phase and redistributes to the mitochondrial matrix at other cell cycle stages.

To determine if total POLID-PTP fluorescence intensity (FI) changed during cell cycle progression, we quantified and compared the FI from individual cells at different cell cycle stages. A small increase in FI was detected in 1N1K$_{div}$ focus-positive cells (Fig. 3B, red bar). However, the increase was not statistically significant compared with 1N1K, 1N1K$_{div}$ focus-negative, 1N2K, and 2N2K cells. To further support this finding, we monitored POLID-PTP protein levels at 60-min intervals following hydroxyurea synchronization (see Fig. S1 in the supplemental material). POLID-PTP protein levels remained constant with no significant differences detected at 1 h after hydroxyurea release when 62% of the population had completed kDNA segregation (1N2K) or at 5 to 7 h when 40% of the population was undergoing kDNA replication, as detected by DAPI staining (see Fig. S1, 1 h).

To confirm the accumulation of POLID-PTP fluorescence within a focus, we quantified the signal ratio of the focus to the mitochondrial matrix from 10 independent cells. To obtain the net FI of the mitochondrial matrix, we subtracted the FI of each focus from the FI of the whole cell (equation 1). The focus FI then was calculated and normalized to the mean FI of the mitochondrial matrix, which revealed that the FI within an individual fluorescent focus increased 4-fold compared to the mitochondrial matrix signal (Fig. 3C). Taken together, these data demonstrate that POLID-PTP focus accumulation results from a redistribution of matrix protein to the kDNA disk and not from a dramatic increase in POLID protein abundance.

The distance between the new and old bb gradually increases through cell cycle progression and provides another indicator for cell cycle stages. Recently, Gull and colleagues provided a detailed examination that demonstrated the tight link between kDNA morphogenesis and bb dynamics (15). They defined five stages (I to V) of the kDNA duplication cycle that differ in kDNA shape, bb and flagellar pocket duplication status, and the presence of antipodal sites. To determine the specific stage during kDNA S phase when POLID-PTP accumulates as foci, we measured the inter-bb distance. Cells with discrete POLID-PTP foci had a minimum distance between the bb of 0.62 μm and a maximum distance of 1.82 μm (Fig. 3D). The mean bb distance for focus-positive cells was 1.1 μm (1.160 ± 0.037; $n = 77$) and 1.3 μm (1.338 ± 0.056; $n = 47$) for cells with no detectable foci (Fig. 3D). Once the bb reached a distance of more than ~2 μm (stage IV), POLID-PTP always localized throughout the mitochondrial matrix (Fig. 3D). These data indicate that POLID-PTP foci accumulate close to the disk only during stages II and III of the kDNA duplication cycle

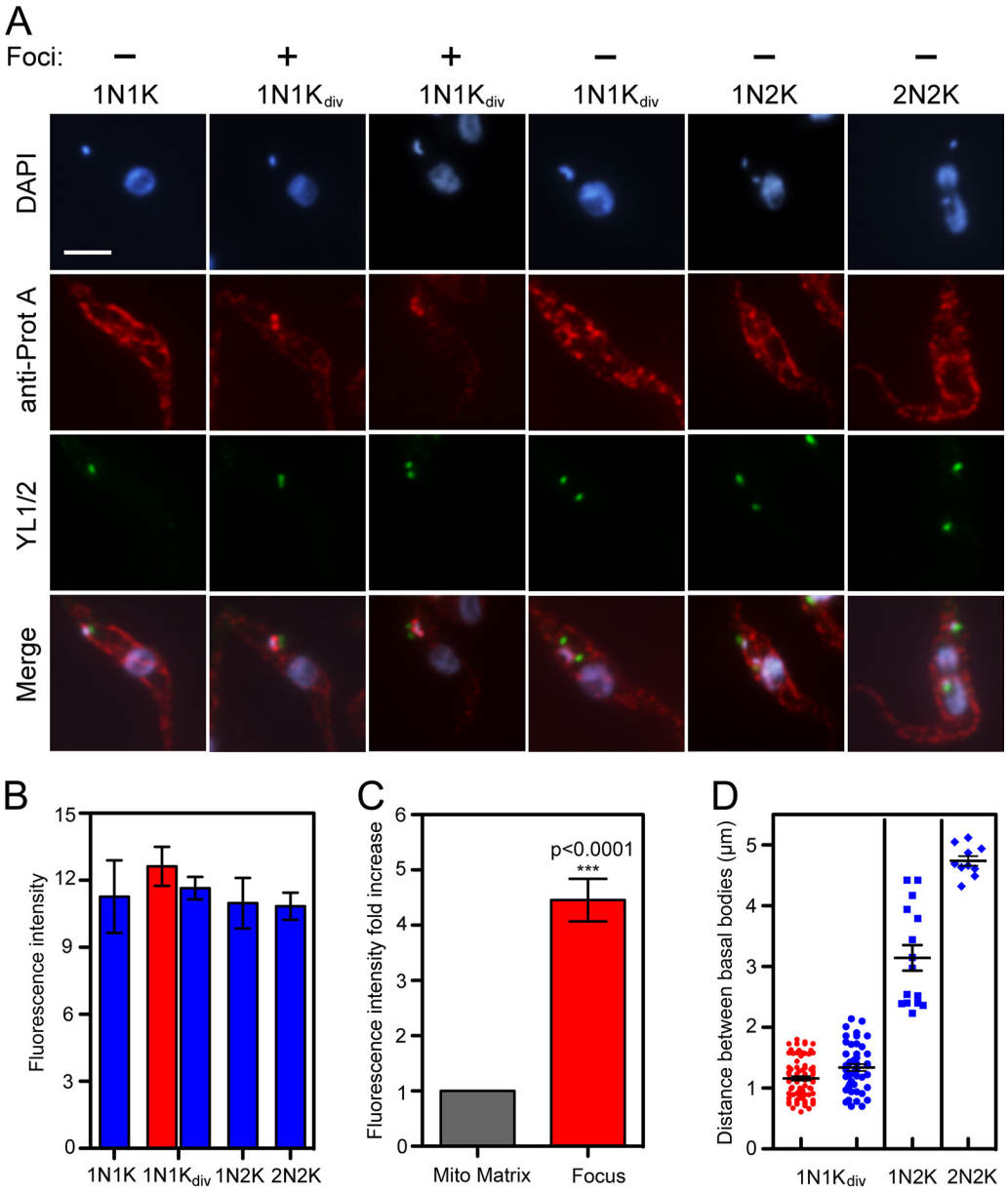

FIG 3 Localization of POLID-PTP during the cell cycle. (A) Representative cells from an unsynchronized population. TbID-PTP cells were dually labeled with anti-protein A that detects POLID-PTP (red) and YL1/2 for the detection of bb (green). DNA was stained with DAPI (blue). Scale bar, 5 μm. (B) Mean fluorescent intensity of POLID-PTP during the cell cycle. The FI was determined in 43 cells at different stages of the cell cycle based on kDNA morphology and bb positioning. The red bar represents cells with POLID-PTP foci. (C) Fold increase in FI of POLID-PTP foci. The net FI of the mitochondrial matrix (gray bar) was calculated and normalized to determine the focus FI fold increase (red bar) (SEM, 4.4 ± 1.21; $n = 10$). (D) Distance between bb during the cell cycle. Measurements are from randomly selected cells ($n = 149$) containing 2 bb/pro-bb pairs with POLID-PTP foci (red) and without foci (blue).

and are characterized by a domed or bilobed network shape and 2 bb/pro-bb pairs. Taken together, these data demonstrate that the redistribution of POLID-PTP from the mitochondrial matrix to foci near the kDNA is tightly coordinated within the 1N1K$_{div}$ *T. brucei* cell cycle stages.

POLID-PTP colocalizes with replicating minicircles at the antipodal sites. Minicircles and maxicircles undergo unidirectional theta replication, and the progeny containing at least one gap then can be labeled with TdT and a fluorescent deoxynucleoside triphosphate (dNTP) (8, 30). Gapped minicircle progeny accumulate at the antipodal sites during kDNA S phase and can be used to distinguish early and late stages of kDNA replication. To precisely define the region of POLID-PTP foci localization and the relationship with replicating minicircles, we fluorescently labeled replicating minicircles and maxicircles using terminal TdT and fluorescein-conjugated dUTP. We detected the same TdT labeling patterns as those previously observed and indicated as early, late, and post-TdT-labeled cells (8). 1N1K cells contained kDNA networks that have not initiated replication and are therefore TdT negative. In these cells, POLID-PTP was dispersed throughout the mitochondrial matrix (Fig. 4A, 1N1K). During early stages of kDNA replication, the antipodal sites are enriched with multiply

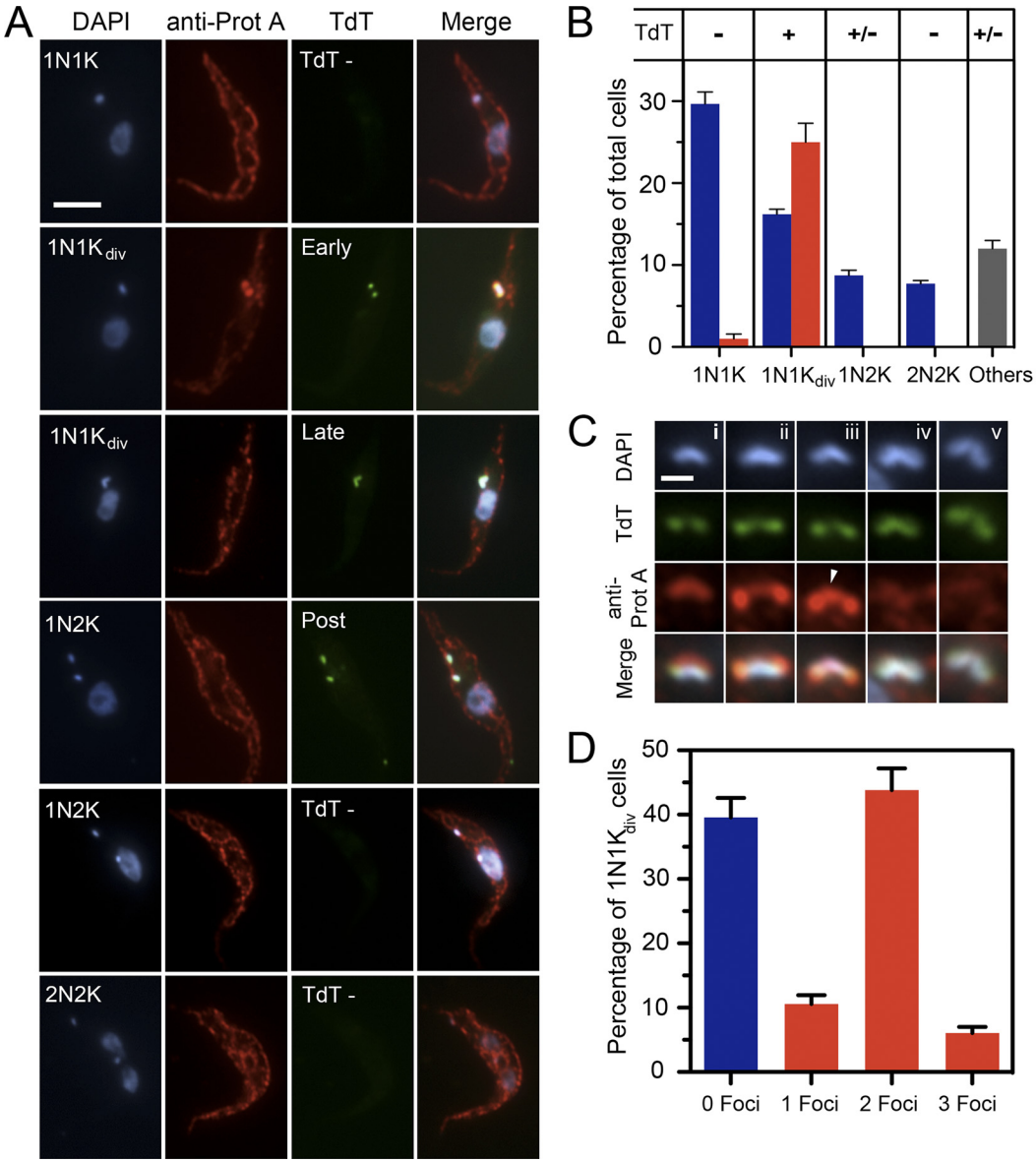

FIG 4 POLID-PTP localization in an asynchronous cell population labeled with TdT. (A) Localization of POLID-PTP relative to the localization of replicating minicircles at the antipodal sites. Scale bar, 5 μm. (B) Distribution of POLID-PTP foci in a population of TdT-labeled cells. Cells were classified based on kDNA morphology and the presence (red bar) or absence (blue bars) of POLID foci. The 1N1K$_{div}$ category included early and late TdT-positive cells. Others (gray bar) included cells with abnormal karyotypes, including multinucleated cells and zoids. (C) Representative images of POLID-PTP foci in 1N1K$_{div}$ TdT-positive cells. (i) Early TdT cells with a single POLID-PTP focus. (ii) Early TdT cells with two distinct POLID-PTP foci. (iii) Early TdT cells with three foci (arrowhead). (iv and v) Late TdT cells with diffuse POLID-PTP signal. Scale bar, 1 μm. (D) The population of 1N1K$_{div}$ cells divided into subcategories based on the number of independent foci per cell.

gapped minicircle intermediates and progeny, resulting in a strong TdT signal at the network poles (Fig. 4A, 1N1K$_{div}$, early TdT). POLID-PTP foci were detected in a subpopulation of the early TdT-positive cells (Fig. 4A, 1N1K$_{div}$). At later stages of kDNA replication (1N1K$_{div}$), the gapped minicircle progeny are reattached to the network, and the signal corresponding to the POLID-PTP foci is diffused, with localization mainly distributed throughout the mitochondrial matrix (Fig. 4A, 1N1K$_{div}$, late TdT). Upon network segregation, a small percentage of the cells are still TdT positive (post-TdT) until all minicircles have completed postreplication gap repair and again become TdT negative. POLID foci were never detected in postreplicating networks (1N2K) or TdT-negative cells.

To determine the percentage of TdT-positive cells that exhibited POLID-PTP foci and confirm that redistribution to the mitochondrial matrix occurred following kDNA replication, we examined ≥300 cells from three separate TdT-labeling experiments and classified them by the presence (red bar) or absence of POLID-PTP foci (blue bars) and kDNA morphology. Cells with a single-unit kinetoplast (1N1K and 1N1K$_{div}$) represented 70% of the TbID-PTP population, with distributions similar to those previously reported in other karyotype analyses (14, 16). Cells with a

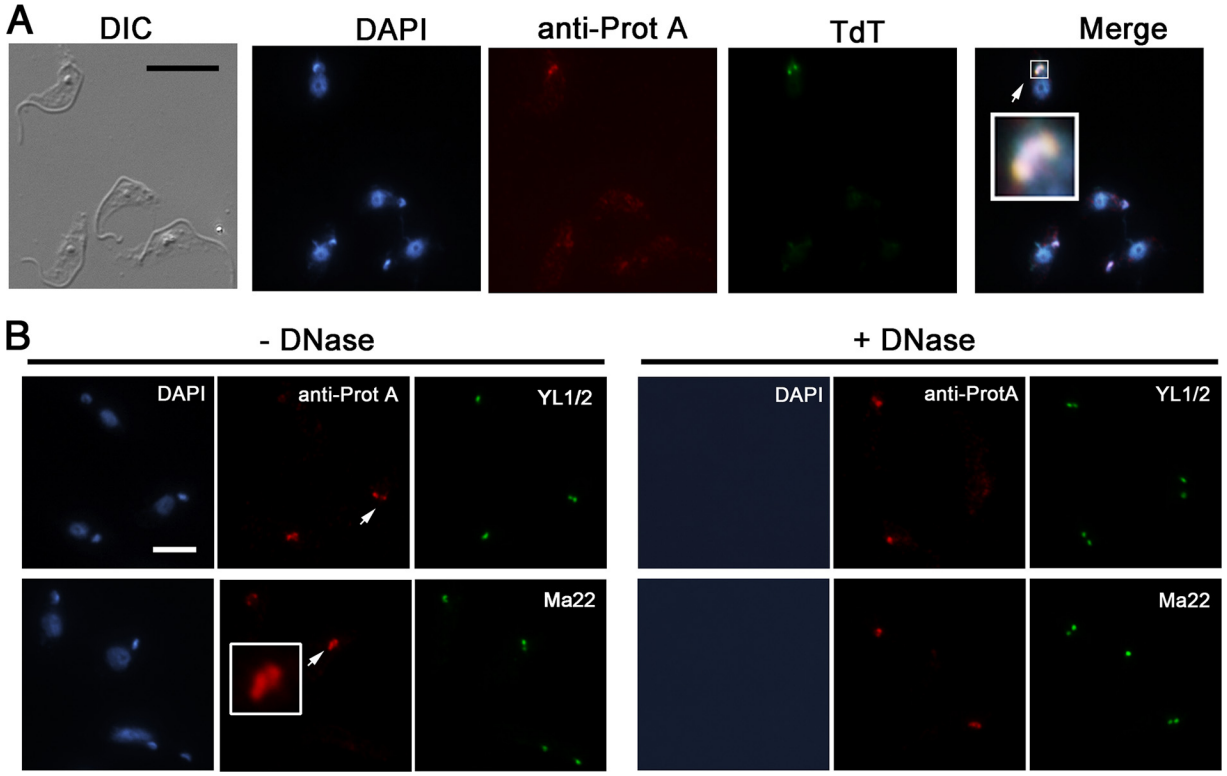

FIG 5 Detection of POLID-PTP foci in extracted cells. (A) Detergent-extracted cells prior to formaldehyde fixation labeled with TdT (green) and anti-protein A (red). Colocalization of POLID-PTP foci with replicating minicircles at the antipodal sites is represented in yellow (merge; see enlargement). Scale bar, 10 μm. (B) Detergent-extracted cells labeled with anti-protein A (red), YL1/2 (green, upper panel), or MAb 22 (green, lower panel). POLID-PTP foci and cytoskeletal components such as basal bodies and exclusion zone filaments were detected in detergent-extracted cells with (+DNase) or without (−DNase) DNase treatment. Three foci also were detected after extraction (enlargement). Scale bar, 5 μm.

single-unit kDNA (1N1K), no TdT signal, and no obvious POLID-PTP foci (Fig. 4B, 1N1K, blue bar) represented 29% of the total population. TdT-positive cells with a single kinetoplast represented 41% of the total population ($1N1K_{div}$, red and blue bars). POLID-PTP foci were detected mainly in $1N1K_{div}$ TdT-positive cells and represented 25% of the total population (Fig. 4B $1N1K_{div}$, red bar). Sixteen percent of the total population was $1N1K_{div}$ TdT positive with no obvious POLID-PTP foci, but they contained mainly mitochondrial matrix signal (Fig. 4B, $1N1K_{div}$, blue bar). POLID-PTP foci were never detected in 1N2K (9%) or 2N2K (8%) cells.

By analyzing the $1N1K_{div}$ TdT-positive fraction of cells more closely, we also observed that cells undergoing kDNA replication displayed different numbers of POLID-PTP foci (Fig. 4C and D). A single focus was observed in 11% of the $1N1K_{div}$ cells, which could represent labeling through the kDNA network or foci too closely positioned to be resolved (Fig. 4Ci and D). Most of the $1N1K_{div}$ cells (44%) contained two independent POLID-PTP foci that colocalized with replicating minicircles at the antipodal sites (Fig. 4Cii and D). Additional images were collected using confocal microscopy, and multiple optical sections were converted to a movie that shows the precise colocalization of POLID-PTP with replicating minicircles (see Movie S1 in the supplemental material, yellow foci). Confocal images were analyzed, and colocalization was confirmed by Pearson's coefficient. One interesting observation was that 6% of cells undergoing kDNA replication had a third focus that accumulated near the center of the network, possibly in the KFZ (Fig. 4Ciii, arrowhead). Most of these cells had a bilobed kDNA, indicating a slightly later stage of kDNA replication. Lastly, 39% of $1N1K_{div}$ cells had no discrete foci in proximity with the kDNA disk; instead, POLID-PTP was detected throughout the mitochondrial matrix (Fig. 4D) and as a faint and diffuse signal across the kDNA network (Fig. 4Civ and v). Taken together, these data demonstrate that POLID-PTP colocalized with replicating minicircles at the antipodal sites specifically during early stages of kDNA S phase.

POLID-PTP foci associate with cytoskeletal elements. The extraction of cells using a nonionic detergent removes soluble and membrane proteins while retaining cytoskeletal elements and DNA-associated proteins. Extraction followed by immunofluorescence has been extensively used to determine that multiple nuclear replication proteins, such as DNA polymerase α and PCNA, are tightly associated with DNA specifically during S phase (48). We used this approach to determine if TbPOLID antipodal localization results from transient binding to kDNA. Cells were extracted with 0.25% NP-40 prior to fixation and then analyzed for the TdT labeling of newly replicated minicircles, POLID-PTP foci, and bb staining. POLID-PTP foci were detected in 20% of the cells following detergent extraction, and these foci colocalized with TdT-positive minicircles at the antipodal sites (Fig. 5A, merge), which is similar to the results obtained with unextracted cells (Fig. 4A). However, the portion of POLID-PTP that localized to the mitochondrial matrix was significantly decreased, suggesting that this fraction of POLID-PTP was solubilized under the extraction

conditions (Fig. 5A). After detergent extraction, cells with 3 foci were also detected (Fig. 5B, −DNase, arrow). POLID-PTP foci are retained along with cytoskeletal elements such as the bb and the exclusion zone filaments even under robust extraction conditions (1% NP-40) (data not shown). To test if the localization of POLID-PTP as discrete foci was dependent on DNA binding, we DNase treated the detergent-extracted cells. After 60 min of DNase treatment, DAPI staining indicated no detectable nuclear DNA or kDNA (even after longer exposure times). Digestion with DNase did not eliminate the POLID-PTP foci, demonstrating that TbPOLID antipodal localization was not the result of transient binding to kDNA (Fig. 5B, +DNase). Cytoskeletal components such as bb and exclusion zone filaments remained intact after detergent extraction and DNase treatment. These data suggest that the specific localization of POLID-PTP foci to the antipodal sites during early stages of kDNA replication is not strictly dependent upon DNA association. Instead, the localization depends mainly upon interactions with cytoskeletal features that persist following extraction.

DISCUSSION

Trypanosome kDNA is the most complex mitochondrial DNA in nature. Important properties include a catenated network composed of minicircles and maxicircles, a single disk-shaped nucleoid structurally linked to the flagellar bb, and an elaborate topoisomerase-mediated release and reattachment mechanism for minicircle replication. Two distinct regions, the antipodal sites and the KFZ, have emerged as important sites for the localization of kDNA replication proteins and minicircle replication intermediates. Previously, we demonstrated that three mitochondrial DNA polymerases (TbPOLIB, TbPOLIC, and TbPOLID) are essential for parasite survival and kDNA replication in both life cycle stages (4–6, 22). While TbPOLIB and TbPOLIC were detected in the KFZ, TbPOLID did not specifically localize near the kDNA disk (22). Given its essential role in kDNA replication, the localization of TbPOLID to the mitochondrial matrix suggested major differences in the mechanism of how this protein engaged in kDNA replication. Here, we provide a detailed examination of TbPOLID localization during the *T. brucei* cell cycle, and we demonstrate that TbPOLID localizes as discrete foci flanking the kDNA disk in a subpopulation of cells (Fig. 1C). Consistently with an essential role in minicircle replication, TbPOLID colocalizes with replicating (gapped) minicircles at the antipodal sites during kDNA replication (Fig. 4A). Importantly, we demonstrated that the major changes in TbPOLID localization occur by the redistribution of this stable protein (Fig. 3C). Because the minicircle replication stages are spatially and temporally separated, the redistribution of TbPOLID represents a mechanism for kDNA replication proteins to participate in this highly coordinated process. This study represents the first detailed characterization of a *T. brucei* kDNA replication protein with dynamic localization during the cell cycle.

Originally, the Okazaki fragment-processing proteins, Pol β and SSE1, as well as $TopoII_{mt}$, were localized to the antipodal sites (12, 13, 32). A great majority of newly identified essential kDNA replication proteins with roles in origin binding, priming, and processive replication also localize to the antipodal sites (p38, p93, PRI1, PRI2, PIF1, and PIF5), suggesting that the role of the antipodal sites is not limited to Okazaki fragment processing. Interestingly, several antipodal site proteins appear to transiently associate with this region, demonstrating that the protein composition is dynamic (20, 43, 46). Studies from the related trypanosome *Crithidia fasiculata* established that the antipodal localization of Pol β and SSE1 correlated with kDNA synthesis and not other cell cycle stages (12, 20). Redistribution was proposed as a mechanism for the localization to the antipodal sites. However, these proteins were undetectable by IF when not present at the antipodal sites, even though protein levels remained constant (12, 20). Here, we provide strong evidence that TbPOLID antipodal localization is due to dynamic redistribution from the mitochondrial matrix in a time-dependent manner during kDNA synthesis. Following kDNA replication, TbPOLID foci disperse from the antipodal sites back to the mitochondrial matrix. The analysis of total TbPOLID FI in individual cells or protein levels in a synchronized population shows that TbPOLID levels remain constant throughout different stages of the cell cycle (Fig. 3A and B; also see Fig. S1 in the supplemental material). Consistent with these data, we show that TbPOLID is highly stable (Fig. 2A), indicating that it is not regulated through proteolytic degradation by the mitochondrial protease HslVU (25). Although POLID levels remained essentially constant, we found a 4-fold increase in FI per TbPOLID focus and a corresponding decrease in FI within the mitochondrial matrix (equation 1). While the majority of TbPOLID is recruited to the antipodal sites and a central focus, approximately 10% remained dispersed in the mitochondrial matrix. It is unclear why a small fraction of TbPOLID is not recruited to the antipodal sites.

Moreover, the recruitment of TbPOLID to the center of the bilobed network was typically associated with stage III of kDNA replication. It was recently confirmed by fluorescent *in situ* hybridization that replicating maxicircles accumulate at the midzone of the network during this stage of kDNA replication (14). It is tempting to speculate that the fraction of POLID concentrated at the midzone plays a role in maxicircle replication. Although our previous data on silencing TbPOLID revealed a role in minicircle replication, the maxicircle copy number declined more rapidly and completely than that of minicircles. These data suggested that POLID also has an important role in maxicircle replication (6). So far, only two proteins have definitive roles in maxicircle replication, the primase PRI1 and the helicase PIF2 (17, 27). Significant questions about maxicircle replication remain unanswered, including what is the maxicircle replicase. Importantly, we have shown that TbPOLID is the first essential mitochondrial DNA polymerase that localizes to the antipodal sites and to the kDNA midzone. However, further studies are required to determine if TbPOLID is a maxicircle replicase or if the central focus represents other POLID functions, such as replication restart or DNA repair.

The multiplicity and spatial separation of the *T. brucei* mitochondrial DNA polymerases suggests that several protein complexes assemble around the kDNA disk (the KFZ and antipodal sites). Others have suggested that the antipodal sites are organized into subdomains populated by different enzyme activities (9, 15). Multiple lines of evidence support this view. First, Okazaki fragment-processing enzymes Pol β and SSE1 appear to colocalize (12), while $TopoII_{mt}$ and Ligk β do not precisely colocalize (9). Second, ethanolic-phosphotungstic acid staining showed regions that differ in staining intensity, indicating the variability of protein concentration in different regions of the antipodal sites (15). The spatial separation of proteins within the antipodal sites could facilitate the formation of functionally different protein complexes.

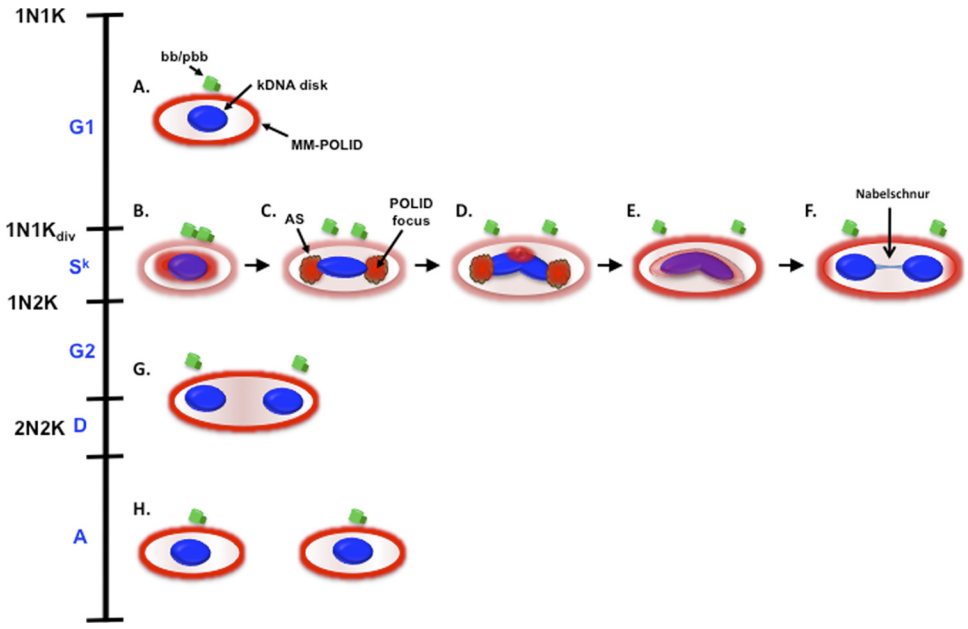

FIG 6 Schematic representation of POLID dynamic localization throughout the *T. brucei* cell cycle. (A) Cells in G_1 (1N1K) with a single kDNA network (blue) with POLID localized throughout the mitochondrial matrix (MM; red). These cells contained a single bb/pro-bb pair (pp/ppb; green). (B) Localization of POLID foci during kDNA duplication cycle (S^k) POLID fluorescence throughout the kDNA disk in cells with a bb/pro-bb pair close together. (C) POLID foci concentrate at the antipodal sites (antipodal sites are shown in brown). (D) A third focus accumulates at the midzone of a bilobe network. (E) Antipodal sites are not visible, and POLID is now detected in the MM. (F) KDNA daughter networks held together by the nabelschnur. POLID is only detected through the MM. (G and H) In 1N2K and 2N2K cells POLID remains dispersed throughout the MM.

Currently we do not know if POLID colocalizes with other kDNA replication proteins or if this polymerase occupies a unique antipodal subdomain. To further understand the dynamics among antipodal site subcomplexes, it will be necessary to identify other components that colocalize with POLID. The existence of subdomains at the antipodal sites suggests that the molecular basis that governs antipodal localization could vary between kDNA replication proteins. So far, the antipodal localization signal is completely unknown.

One possible mechanism for the stable association of protein to the antipodal sites is by a direct or indirect association with cytoskeletal elements. The KFZ is traversed by structural filaments that form part of the TAC and link the kDNA disk to the bb to control network segregation. It is possible that similar structural elements traverse the antipodal sites to give stability to protein complexes that localize to subdomains in this region. While no structural elements have been definitively characterized for the antipodal sites, differential cytochemical staining and electron microscopic analyses revealed fibrous structures at the antipodal sites that stain differently from the inner unilateral filaments of the TAC, suggesting different cytoskeletal elements (15). Alternatively, these could protect this highly specific region, where replication intermediates are detected from other processes occurring in the MM. Intriguingly, we show that the dynamics of TbPOLID foci were not dependent on membranous structures or other soluble proteins following detergent extraction. TbPOLID and replicating (gapped) minicircles colocalized at the antipodal sites even following detergent extraction with stringent conditions (Fig. 5A). These data suggest that cytoskeletal elements play a role in the stable association of proteins and DNA to the antipodal sites. Consistent with these findings, we demonstrate that TbPOLID antipodal localization was not affected in the absence of DNA (Fig. 5C). A specialized mitochondrial nucleoid-associated structure is also present in yeast mitochondria (31). The anchoring of yeast nucleoids to the cytoskeleton through Mgm1p and Mmm1p is essential not only for segregation and inheritance but also for replication. Interestingly, the yeast mitochondrial DNA polymerase Mip1 is a stable component of this structure (31). Additionally, mammalian mtDNA foci are associated with cytoskeletal elements, as they remained stable after membranes and soluble components were extracted (19). This association is maintain by KIF5B, the kinesin motor protein implicated in moving mitochondria along microtubules (19). The identification of the link between the antipodal sites and a cytoskeletal component will help us understand how minicircle replication intermediates and kDNA replication proteins assume such a defined localization pattern.

The coordination of proteins involved in early and later stages of kDNA replication is a fundamental yet poorly understood process. The intramitochondrial localization of kDNA replication proteins has provided a framework for the current model of kDNA replication and has been important for formulating new hypotheses. Our study represents a significant step toward understanding the spatial and temporal coordination of proteins during kDNA replication stages. All of the changes determined from images and the quantification of the TbPOLID dynamic redistribution (Fig. 3 and 4) are summarized schematically in Fig. 6. During G_1 phase, cells contain a single bb/pro-bb pair, prereplication kDNA networks with covalently closed minicircles and maxicircles that do not label with TdT, and POLID fluorescence that is detected throughout the mitochondrial matrix (Fig. 6A). Upon entering kDNA S phase, a small percentage of cells display POLID

fluorescence throughout the kDNA disk (Fig. 6B), and then POLID colocalizes at two independent foci with minicircle replication intermediates (labeled with TdT), as they accumulate mainly at the antipodal sites, and the kinetoplast is associated with two bb/pro-bb pairs (Fig. 6C). As kDNA replication progresses and the network elongates to form a bilobed structure, POLID remains associated with the antipodal sites while a third focus accumulates at the center of the stage III kinetoplast (Fig. 6D). At this time point the gapped minicircles are still associated with the antipodal sites. Subsequently, the cell enters into a postreplicative stage, where gapped minicircles are detected throughout the kDNA disk and the POLID fluorescence is no longer focused in spots but instead is diffuse throughout the kDNA disk, and it appears to redistribute to the mitochondrial matrix (Fig. 6E). The kinetoplast then enters stage IV, where 2-unit-sized disks have moved apart (1.68 μm) (14) but are still connected by the nabelschnur (Fig. 6F). At this stage there are no longer any free minicircle replication intermediates detected, and POLID has nearly completed redistribution to the mitochondrial matrix. The kinetoplasts continue to separate as the cell completes mitosis and undergoes cell division. During these postreplicative stages, POLID is always found distributed in the mitochondrial matrix (Fig. 6G and H) until the next round of kDNA synthesis begins.

ACKNOWLEDGMENTS

This work was supported by NIH grant RO1 AI066279 to M.M.K. J.C.A. was supported through the Northeast Alliance for Graduate Education and the Professoriate Program (NEAGEP), funded by NSF grant 0450339.

We are grateful to Paul Englund for Hsp70 and Pol β antibodies and Derrick R. Robinson for MAb 22 sera. We also thank Arthur Günzl for the pPTP-NEO vector and advice. We also thank David Bruhn, Eva Gluenz, and Tina Saxowsky for the critical reading of the manuscript. Lastly, we thank Louise Bertrand from Leica for assistance with confocal microscopy and Dale Callaham from the University of Massachusetts, Amherst, microscopy core facility for much advice.

REFERENCES

1. **Bogenhagen DF, Rousseau D, Burke S.** 2008. The layered structure of human mitochondrial DNA nucleoids. J. Biol. Chem. **283**:3665–3675.
2. **Boldogh IR, et al.** 2003. A protein complex containing Mdm10p, Mdm12p, and Mmm1p links mitochondrial membranes and DNA to the cytoskeleton-based segregation machinery. Mol. Biol. Cell **14**:4618–4627.
3. **Bonhivers M, Landrein N, Decossas M, Robinson DR.** 2008. A monoclonal antibody marker for the exclusion-zone filaments of Trypanosoma brucei. Parasit. Vectors **1**:21.
4. **Bruhn DF, Mozeleski B, Falkin L, Klingbeil MM.** 2010. Mitochondrial DNA polymerase POLIB is essential for minicircle DNA replication in African trypanosomes. Mol. Microbiol. **75**:1414–1425.
5. **Bruhn DF, Sammartino MP, Klingbeil MM.** 2011. Three mitochondrial DNA polymerases are essential for kinetoplast DNA replication and survival of bloodstream form Trypanosoma brucei. Eukaryot. Cell **10**:734–743.
6. **Chandler J, Vandoros AV, Mozeleski B, Klingbeil MM.** 2008. Stem-loop silencing reveals that a third mitochondrial DNA polymerase, POLID, is required for kinetoplast DNA replication in trypanosomes. Eukaryot. Cell **7**:2141–2146.
7. **Chen XJ, Butow RA.** 2005. The organization and inheritance of the mitochondrial genome. Nat. Rev. Genet. **6**:815–825.
8. **Chowdhury AR, Zhao Z, Englund PT.** 2008. Effect of hydroxyurea on procyclic Trypanosoma brucei: an unconventional mechanism for achieving synchronous growth. Eukaryot. Cell **7**:425–428.
9. **Downey N, Hines JC, Sinha KM, Ray DS.** 2005. Mitochondrial DNA ligases of Trypanosoma brucei. Eukaryot. Cell **4**:765–774.
10. **Drew ME, Englund PT.** 2001. Intramitochondrial location and dynamics of Crithidia fasciculata kinetoplast minicircle replication intermediates. J. Cell Biol. **153**:735–744.
11. **Effron PN, Torri AF, Engman DM, Donelson JE, Englund PT.** 1993. A mitochondrial heat shock protein from Crithidia fasciculata. Mol. Biochem. Parasitol. **59**:191–200.
12. **Engel ML, Ray DS.** 1999. The kinetoplast structure-specific endonuclease I is related to the 5′ exo/endonuclease domain of bacterial DNA polymerase I and colocalizes with the kinetoplast topoisomerase II and DNA polymerase beta during replication. Proc. Natl. Acad. Sci. U. S. A. **96**:8455–8460.
13. **Ferguson ML, Torri AF, Perez-Morga D, Ward DC, Englund PT.** 1994. Kinetoplast DNA replication: mechanistic differences between Trypanosoma brucei and Crithidia fasciculata. J. Cell Biol. **126**:631–639.
14. **Gluenz E, Povelones ML, Englund PT, Gull K.** 2011. The kinetoplast duplication cycle in Trypanosoma brucei is orchestrated by cytoskeleton-mediated cell morphogenesis. Mol. Cell. Biol. **31**:1012–1021.
15. **Gluenz E, Shaw MK, Gull K.** 2007. Structural asymmetry and discrete nucleic acid subdomains in the Trypanosoma brucei kinetoplast. Mol. Microbiol. **64**:1529–1539.
16. **Hammarton TC, Kramer S, Tetley L, Boshart M, Mottram JC.** 2007. Trypanosoma brucei Polo-like kinase is essential for basal body duplication, kDNA segregation and cytokinesis. Mol. Microbiol. **65**:1229–1248.
17. **Hines JC, Ray DS.** 2010. A mitochondrial DNA primase is essential for cell growth and kinetoplast DNA replication in Trypanosoma brucei. Mol. Cell. Biol. **30**:1319–1328.
18. **Hines JC, Ray DS.** 2011. A second mitochondrial DNA primase is essential for cell growth and kinetoplast minicircle DNA replication in Trypanosoma brucei. Eukaryot. Cell **10**:445–454.
19. **Iborra FJ, Kimura H, Cook PR.** 2004. The functional organization of mitochondrial genomes in human cells. BMC Biol. **2**:9.
20. **Johnson CE, Englund PT.** 1998. Changes in organization of Crithidia fasciculata kinetoplast DNA replication proteins during the cell cycle. J. Cell Biol. **143**:911–919.
21. **Kaufman BA, et al.** 2000. In organello formaldehyde crosslinking of proteins to mtDNA: identification of bifunctional proteins. Proc. Natl. Acad. Sci. U. S. A. **97**:7772–7777.
22. **Klingbeil MM, Motyka SA, Englund PT.** 2002. Multiple mitochondrial DNA polymerases in Trypanosoma brucei. Mol. Cell **10**:175–186.
23. **Kucej M, Kucejova B, Subramanian R, Chen XJ, Butow RA.** 2008. Mitochondrial nucleoids undergo remodeling in response to metabolic cues. J. Cell Sci. **121**:1861–1868.
24. **Lamb JR, Fu V, Wirtz E, Bangs JD.** 2001. Functional analysis of the trypanosomal AAA protein TbVCP with trans-dominant ATP hydrolysis mutants. J. Biol. Chem. **276**:21512–21520.
25. **Li Z, Lindsay ME, Motyka SA, Englund PT, Wang CC.** 2008. Identification of a bacterial-like HslVU protease in the mitochondria of Trypanosoma brucei and its role in mitochondrial DNA replication. PLoS Pathog. **4**:e1000048.
26. **Liu B, et al.** 2006. Role of p38 in replication of Trypanosoma brucei kinetoplast DNA. Mol. Cell. Biol. **26**:5382–5393.
27. **Liu B, et al.** 2009. Trypanosomes have six mitochondrial DNA helicases with one controlling kinetoplast maxicircle replication. Mol. Cell **35**:490–501.
28. **Liu B, Wang J, Yildirir G, Englund PT.** 2009. TbPIF5 is a Trypanosoma brucei mitochondrial DNA helicase involved in processing of minicircle Okazaki fragments. PLoS Pathog. **5**:e1000589.
29. **Liu B, et al.** 2010. TbPIF1, a Trypanosoma brucei mitochondrial DNA helicase, is essential for kinetoplast minicircle replication. J. Biol. Chem. **285**:7056–7066.
30. **Liu Y, Motyka SA, Englund PT.** 2005. Effects of RNA interference of Trypanosoma brucei structure-specific endonuclease-I on kinetoplast DNA replication. J. Biol. Chem. **280**:35513–35520.
31. **Meeusen S, Nunnari J.** 2003. Evidence for a two membrane-spanning autonomous mitochondrial DNA replisome. J. Cell Biol. **163**:503–510.
32. **Melendy T, Sheline C, Ray DS.** 1988. Localization of a type II DNA topoisomerase to two sites at the periphery of the kinetoplast DNA of Crithidia fasciculata. Cell **55**:1083–1088.
33. **Milman N, Motyka SA, Englund PT, Robinson D, Shlomai J.** 2007. Mitochondrial origin-binding protein UMSBP mediates DNA replication and segregation in trypanosomes. Proc. Natl. Acad. Sci. U. S. A. **104**:19250–19255.
34. **Motyka SA, Drew ME, Yildirir G, Englund PT.** 2006. Overexpression of a cytochrome b5 reductase-like protein causes kinetoplast DNA loss in Trypanosoma brucei. J. Biol. Chem. **281**:18499–18506.
35. **Nunnari J, et al.** 1997. Mitochondrial transmission during mating in Saccharomyces cerevisiae is determined by mitochondrial fusion and fis-

sion and the intramitochondrial segregation of mitochondrial DNA. Mol. Biol. Cell **8**:1233–1242.
36. **Oberholzer M, Morand S, Kunz S, Seebeck T.** 2006. A vector series for rapid PCR-mediated C-terminal in situ tagging of Trypanosoma brucei genes. Mol. Biochem. Parasitol. **145**:117–120.
37. **Ochsenreiter T, Anderson S, Wood ZA, Hajduk SL.** 2008. Alternative RNA editing produces a novel protein involved in mitochondrial DNA maintenance in trypanosomes. Mol. Cell. Biol. **28**:5595–5604.
38. **Ogbadoyi EO, Robinson DR, Gull K.** 2003. A high-order transmembrane structural linkage is responsible for mitochondrial genome positioning and segregation by flagellar basal bodies in trypanosomes. Mol. Biol. Cell **14**:1769–1779.
39. **Pohjoismaki JL, et al.** 2009. Human heart mitochondrial DNA is organized in complex catenated networks containing abundant four-way junctions and replication forks. J. Biol. Chem. **284**:21446–21457.
40. **Pradel LC, Bonhivers M, Landrein N, Robinson DR.** 2006. NIMA-related kinase TbNRKC is involved in basal body separation in Trypanosoma brucei. J. Cell Sci. **119**:1852–1863.
41. **Robinson DR, Gull K.** 1991. Basal body movements as a mechanism for mitochondrial genome segregation in the trypanosome cell cycle. Nature **352**:731–733.
42. **Robinson DR, Sherwin T, Ploubidou A, Byard EH, Gull K.** 1995. Microtubule polarity and dynamics in the control of organelle positioning, segregation, and cytokinesis in the trypanosome cell cycle. J. Cell Biol. **128**:1163–1172.
43. **Saxowsky TT, Choudhary G, Klingbeil MM, Englund PT.** 2003. Trypanosoma brucei has two distinct mitochondrial DNA polymerase beta enzymes. J. Biol. Chem. **278**:49095–49101.
44. **Schimanski B, Nguyen TN, Gunzl A.** 2005. Highly efficient tandem affinity purification of trypanosome protein complexes based on a novel epitope combination. Eukaryot. Cell **4**:1942–1950.
45. **Sela D, et al.** 2008. Unique characteristics of the kinetoplast DNA replication machinery provide potential drug targets in trypanosomatids. Adv. Exp. Med. Biol. **625**:9–21.
46. **Sinha KM, Hines JC, Ray DS.** 2006. Cell cycle-dependent localization and properties of a second mitochondrial DNA ligase in Crithidia fasciculata. Eukaryot. Cell **5**:54–61.
47. **Spelbrink JN.** 2010. Functional organization of mammalian mitochondrial DNA in nucleoids: history, recent developments, and future challenges. IUBMB Life **62**:19–32.
48. **Stokke T, Erikstein B, Holte H, Funderud S, Steen HB.** 1991. Cell cycle-specific expression and nuclear binding of DNA polymerase alpha. Mol. Cell. Biol. **11**:3384–3389.
49. **Stuart KD, Schnaufer A, Ernst NL, Panigrahi AK.** 2005. Complex management: RNA editing in trypanosomes. Trends Biochem. Sci. **30**:97–105.
50. **Wang Z, Englund PT.** 2001. RNA interference of a trypanosome topoisomerase II causes progressive loss of mitochondrial DNA. EMBO J. **20**:4674–4683.
51. **Woodward R, Gull K.** 1990. Timing of nuclear and kinetoplast DNA replication and early morphological events in the cell cycle of Trypanosoma brucei. J. Cell Sci. **95**:49–57.
52. **Zhao Z, Lindsay ME, Roy Chowdhury A, Robinson DR, Englund PT.** 2008. p166, a link between the trypanosome mitochondrial DNA and flagellum, mediates genome segregation. EMBO J. **27**:143–154.